



Characterization of material mechanical properties using strain correlation method combined with virtual fields method

Yangyang Li¹ · Jiaqiang Li¹ · Qiyuan Duan¹ · Huimin Xie¹ · Sheng Liu^{2,3}

Received: 26 May 2020 / Revised: 12 September 2020 / Accepted: 2 October 2020 / Published online: 7 January 2021
© The Chinese Society of Theoretical and Applied Mechanics and Springer-Verlag GmbH Germany, part of Springer Nature 2021

Abstract

The isotropic and anisotropic behaviors are considered as the important formats of the constitutive behaviors, and can also be called the global properties. To improve the identification ability of virtual fields method (VFM) when the global properties are unknown, this paper proposes the strain correlation method (SCM) to determine the global properties before the parameter identification using the VFM. Firstly, the basic principle of SCM is described in detail. Then, the feasibility and accuracy of SCM are verified through the numerical experiments based on the three-point bending configuration and the real experiment of polymethyl methacrylate (PMMA). The influence of the additive Gaussian white noise, local errors in the strain fields, and missing data at the specimen edges on the characterization results are evaluated. The results show that the SCM has good noise immunity and lower accuracy requirements for the strain fields. As an application, the mechanical properties of Ti-6Al-4V alloys fabricated by selective laser melting (SLM) are characterized by the SCM. The results show that the alloys are isotropic, and the isotropic VFM is utilized to determine the mechanical parameters. By using the SCM, the accuracy of identification results can be improved for the isotropic or bidirectional reinforced orthotropic materials when using VFM.

Keywords Global properties · Constitutive parameter identification · Strain correlation method · Virtual fields method

1 Introduction

Characterization of material mechanical properties is a significant and challenging task in experimental solid mechanics [1, 2]. Generally, there are two main approaches to identify the mechanical parameters governing the constitutive equations: one is based on the standard tests (using strain gauges or extensometer), the other is based on the full-field measurement technology. The former requires homogeneous strain or stress state, however, when the constitutive behav-

iors are complex, a large number of experiments are required. The development of full-field measurement technology provides another way for multi-parameter identification [3]. To achieve the multi-parameter identification, various identification methods have been proposed, including the finite element model updating (FEMU) [4, 5], the constitutive equation gap method (CEGM) [6, 7], and the equilibrium gap method (EGM) [8]. For both elastic and inelastic properties, these methods are to establish a constrained optimization equation and then use the iterative algorithm to obtain the unknown parameters [9, 10]. Before the iterative calculation, the initial values of the unknown parameters need to be determined. The setting of the initial value will affect the speed of calculation convergence and the accuracy of the results.

In recent years, a novel identification strategy named the virtual fields method (VFM) has been widely studied [11, 12]. The VFM is a non-iterative method for the linear elastic situation, and the current full-field measurement techniques combined with VFM include the digital image correlation (DIC) [13], moiré interferometry [14], grid method [15], etc. The VFM has been widely applied in various materials, such as composite materials [16], laser weldments [17], and additive manufacturing materials [18–20]. In the case of

Executive Editor: Xing-Long Gong

✉ Huimin Xie
xiehm@mail.tsinghua.edu.cn

✉ Sheng Liu
victor_liu63@vip.126.com

¹ School of Aerospace Engineering, Tsinghua University, Beijing 100084, China

² Institute of Technological Sciences, Wuhan University, Wuhan 430072, China

³ Lab for Hydropower Transients of Ministry of Education, School of Power and Mechanical Engineering, Wuhan University, Wuhan 430072, China

linear elasticity, it has been applied in various constitutive models including but not limited to isotropic elasticity [11], transverse isotropic elasticity [21], orthotropic elasticity [16] and orthotropic thermo-elasticity [22]. For orthotropic VFM, due to the increase in the number of unknown parameters, many factors will affect the accuracy of identification results, including noises in the strain fields [23], selection of virtual fields [24], loading configuration [20, 25], etc.

However, when using these identification methods, the material constitutive behaviors or global properties are known as priors. Generally, if the material global properties are unknown, it can be assumed to be anisotropic, and then all parameters are identified, and finally, according to the relationship between the parameters, the global properties can be determined. For planar problems, for example, the orthotropic VFM (four unknown parameters: Q_{11} , Q_{22} , Q_{12} and Q_{66} , subscript “1”, “2” mean along the material principal axis) can be directly applied to identify all parameters. If the parameters satisfy with the relationship $Q_{11} = Q_{22}$ and $Q_{66} = (Q_{11} - Q_{12})/2$, then the material is isotropic. If the parameters only satisfy with the relationship $Q_{11} = Q_{22}$, then it is bidirectional reinforced orthotropic, otherwise, it is completely orthotropic. However, many factors affect the identification accuracy of orthotropic VFM, it may be laborious to fully consider these factors [20, 23–25]. In addition, to obtain each parameter precisely requires that all strain fields can be measured accurately, which is very difficult in real experiments. Therefore, for isotropic and bidirectional reinforced orthotropic materials, the above-mentioned method may lead to incorrect determination of the global properties. To handle these issues, this study aims to introduce a simple method with low accuracy requirements for the strain fields to determine the material global properties before using VFM.

In this study, the strain correlation method (SCM) is proposed to determine the material global properties before using VFM. In the theory section, the principle of SCM and VFM is illustrated in detail. Then, the feasibility and accuracy of the SCM are verified by numerical experiments based on the three-point bending configuration. The influencing factors including the additive Gaussian white noise, local errors in strain fields, and missing data at the specimen edges are discussed by numerical experiments. Furthermore, the comparative studies of SCM and orthotropic VFM are also conducted to illustrate the robustness of SCM. In the experiment section, the verification experiment using polymethyl methacrylate (PMMA) is conducted to illustrate the feasibility of SCM in real experiments. After that, the Ti-6Al-4V alloys fabricated by alternative cross routes are characterized by SCM and VFM. The results are reasonable compared with those in the literature.

2 Theory

2.1 Principle of SCM

Considering the planar problem, there are three strain fields ϵ_{xx} , ϵ_{yy} and γ_{xy} . Taking the strain field ϵ_{xx} as an example. The SCM is to determine the material global properties by performing correlation calculation between the experimental strain field (ϵ_{xx}^{exp}) and a series of simulated strain fields. First, two kinds of strain libraries (L_{iso}^{simu} , L_{orth}^{simu}) are established using the finite element method, one strain library contains strain fields with n different isotropic materials ($L_{iso}^{simu} = \{\epsilon_{iso-1}^{simu}, \epsilon_{iso-2}^{simu}, \dots, \epsilon_{iso-n}^{simu}\}$, n is a positive integer), and the other contains strain fields with n different orthotropic materials ($L_{orth}^{simu} = \{\epsilon_{orth-1}^{simu}, \epsilon_{orth-2}^{simu}, \dots, \epsilon_{orth-n}^{simu}\}$). Then, the experimental strain field (ϵ_{xx}^{exp}) is correlated with the libraries, and two groups of the coefficients ($C_{iso} = \{C_{iso}^1, C_{iso}^2, \dots, C_{iso}^n\}$, $C_{orth} = \{C_{orth}^1, C_{orth}^2, \dots, C_{orth}^n\}$) are obtained. Finally, after comparing the two groups of coefficients, according to which group has the maximum number of the maximum coefficients, the material global properties can be determined. The schematic of the SCM is shown in Fig. 1.

For the planar problem, the strain fields can be stored as a matrix in the computer, which facilitates correlation calculation. Due to this convenience, both the experimental strain fields and the strain fields in strain libraries are stored as matrices. Therefore, the correlation calculation of the strain fields is equivalent to that of the matrices. Through the correlation calculation, the similarity of the global properties of the strain fields can be compared. In matrix correlation analysis, there are various calculation indicators to characterize the correlation between the two matrices. In this paper, the algorithm for calculating the correlation coefficient is as follows [26]:

$$r = \frac{\sum_m \sum_n (A_{mn} - \bar{A})(B_{mn} - \bar{B})}{\sqrt{[\sum_m \sum_n (A_{mn} - \bar{A})^2][\sum_m \sum_n (B_{mn} - \bar{B})^2]}}$$

$$r \in [-1, 1], \tag{1}$$

where r is the correlation coefficient of matrix A and matrix B , m and n represent the number of rows and columns, respectively. \bar{A} and \bar{B} represent the average value of the whole matrix A and B , respectively. In this paper, matrices A and B represent the experimental strain field and strain field in strain libraries, respectively.

2.2 Theory of VFM

VFM is based on the principle of virtual work [11]. When the volume forces and acceleration terms are not considered,

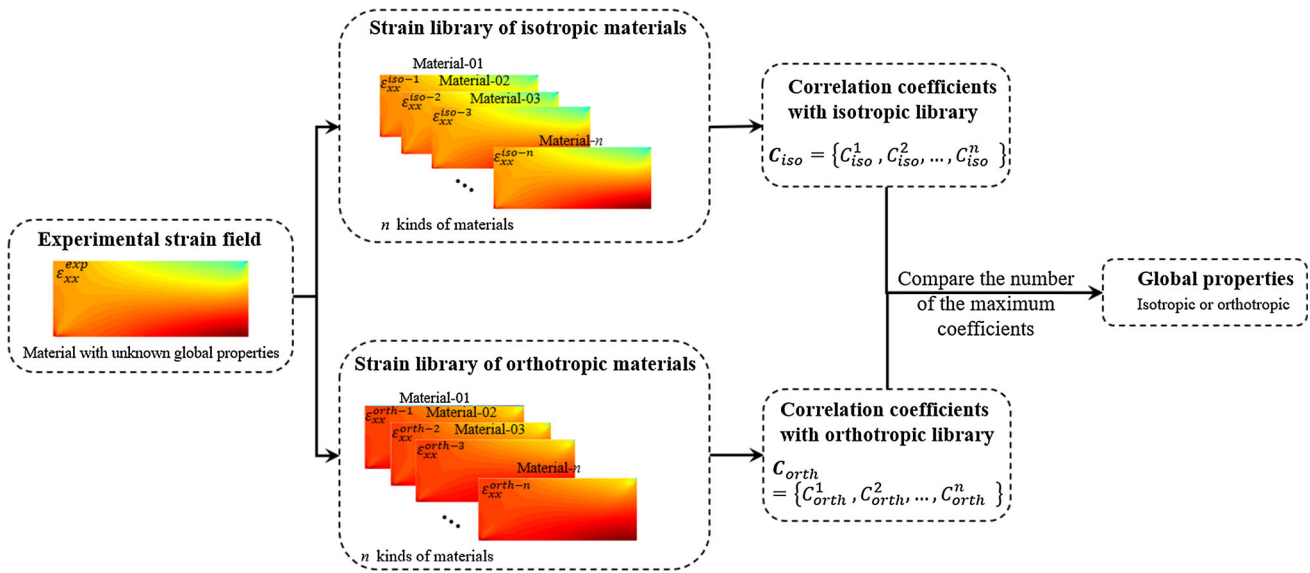


Fig. 1 Schematic diagram of the SCM (taking the strain field ϵ_{xx} as an example)

suppose the volume of the object is V , the external surface area is S , and the external load vector on the surface is \bar{T} , the governing equation of VFM is as follows [11]:

$$-\int_V \sigma : \epsilon^* dV + \int_S \bar{T} \cdot u^* dS = 0, \quad \forall u^* \in KA, \quad (2)$$

where σ is the stress tensor, ϵ^* is the virtual strain field, u^* is the virtual displacement field, and KA means kinematically admissible conditions.

In the case of orthotropic materials, the constitutive equation under the principal axis (with subscript “1”, “2”) can be expressed by Eq. (3) [11]:

$$\begin{Bmatrix} \sigma_{11} \\ \sigma_{22} \\ \sigma_{12} \end{Bmatrix} = \begin{bmatrix} Q_{11} & Q_{12} & 0 \\ Q_{12} & Q_{22} & 0 \\ 0 & 0 & Q_{66} \end{bmatrix} \begin{Bmatrix} \epsilon_{11} \\ \epsilon_{22} \\ \gamma_{12} \end{Bmatrix}, \quad (3)$$

where Q_{ij} ($i, j = 1, 2, 6$) are the four stiffness parameters. Bring Eq. (3) into Eq. (2) to get Eq. (4) [11]:

$$\begin{aligned} & Q_{11}t \int_S \underbrace{\epsilon_{11}\epsilon_{11}^*}_{A} dS + Q_{22}t \int_S \underbrace{\epsilon_{22}\epsilon_{22}^*}_{B} dS + Q_{12}t \int_S \underbrace{(\epsilon_{11}\epsilon_{22}^* + \epsilon_{22}\epsilon_{11}^*)}_{C} dS \\ & + Q_{66}t \int_S \underbrace{\gamma_{12}\gamma_{12}^*}_{D} dS = \int_S \bar{T} \cdot u^* dS, \quad \forall u^* \in KA, \end{aligned} \quad (4)$$

where t is the thickness of the specimen.

In Eq. (4), four parameters are unknown, therefore four independent virtual fields need to be determined. Considering the special virtual fields in Ref. [11], for each virtual field, the coefficients $[A, B, C, \text{ and } D]$ in Eq. (4) of three of the four unknown parameters are zero, and the other one is unity.

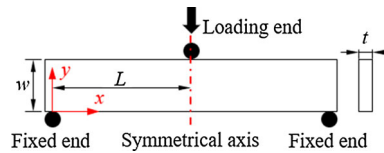


Fig. 2 Three-point bending configuration

For more details, refer to Refs. [11, 24]. Furthermore, the selection of the virtual fields is also an important factor in the identification. In this paper, the optimized polynomial virtual fields are used [11]:

$$\begin{cases} u_x^* = \sum_{i=0}^p \sum_{j=0}^q A_{ij} \left(\frac{x}{L}\right)^i \left(\frac{y}{w}\right)^j, \\ u_y^* = \sum_{i=0}^p \sum_{j=0}^q B_{ij} \left(\frac{x}{L}\right)^i \left(\frac{y}{w}\right)^j, \end{cases} \quad (5)$$

where p, q are the orders of the polynomials, A_{ij}, B_{ij} are the coefficients of the polynomials, which can be optimized by the algorithm [11], and L, w are the span and height of the specimen, as shown in Fig. 2.

In the case of isotropic materials, the stiffness parameters have the following relation: $Q_{11} = Q_{22}, Q_{66} = (Q_{11} - Q_{12})/2$. Accordingly, Eq. (4) can be written as:

$$\begin{aligned} & Q_{11}t \int_S \underbrace{(\epsilon_{11}\epsilon_{11}^* + \epsilon_{22}\epsilon_{22}^* + \frac{1}{2}\gamma_{12}\gamma_{12}^*)}_{E} dS \\ & + Q_{12}t \int_S \underbrace{(\epsilon_{11}\epsilon_{22}^* + \epsilon_{22}\epsilon_{11}^* - \frac{1}{2}\gamma_{12}\gamma_{12}^*)}_{F} dS \\ & = \int_S \bar{T} \cdot u^* dS, \quad \forall u^* \in KA, \end{aligned} \quad (6)$$

where the subscript “1” corresponds to “x”, and the subscript “2” corresponds to “y”.

Given that the shear strain of the three-point bending is smaller than ϵ_{11} and ϵ_{22} , to weaken the influence of shear strain on the identification of the other two parameters (Q_{11} and Q_{12}), the governing equation is rewritten as:

$$Q_{11}t \int_S \overbrace{(\epsilon_{11}\epsilon_{11}^* + \epsilon_{22}\epsilon_{22}^*)}^H dS + Q_{12}t \int_S \overbrace{(\epsilon_{11}\epsilon_{22}^* + \epsilon_{22}\epsilon_{11}^*)}^I dS + Q_{66}t \int_S \overbrace{\gamma_{12}\gamma_{12}^*}^J dS = \int_S \bar{T} \cdot u^* dS, \quad \forall u^* K A. \quad (7)$$

Equation (7) does not consider $Q_{66} = (Q_{11} - Q_{12})/2$, this relationship is used to calculate Q_{66} after obtaining Q_{11} and Q_{12} . This purpose is to reduce the influence of the shear strain field on other parameters for the isotropic case. Furthermore, the optimized polynomial virtual fields are used for isotropic VFM [11].

In addition, as shown in Fig. 2, the loading configuration is symmetrical, so the boundary conditions are set as follows: the virtual displacement in the x -direction is restricted on the symmetry axis, and the virtual displacement in the y -direction is constant. The virtual displacements of the fixed end are zero. The specific expression is as follows:

$$\begin{cases} u_x^*(L, y) = 0, \\ u_y^*(L, y) = \text{const.}, \\ u_x^*(0, 0) = 0, \\ u_y^*(0, 0) = 0. \end{cases} \quad (8)$$

The theory of SCM and VFM has been described in detail above. Conclusively, for materials with unknown constitutive behaviors, the SCM is used to determine the global properties, and then VFM is performed for parameter identification. The flowchart of the SCM-VFM is shown in Fig. 3.

3 Verification of SCM

3.1 Simulation results of SCM with additive Gaussian white noise

In this section, the feasibility of the SCM will be verified by numerical methods. The simulation model is built in ABAQUS, as shown in Fig. 4. The L and w are 24 mm and 8 mm respectively. The thickness is 2 mm, and the element type is CPS4.

According to the procedure in Fig. 3, the isotropic and orthotropic strain library should be established. The primary problem is how to select the constitutive parameters of the two kinds of strain libraries, and then how to obtain these

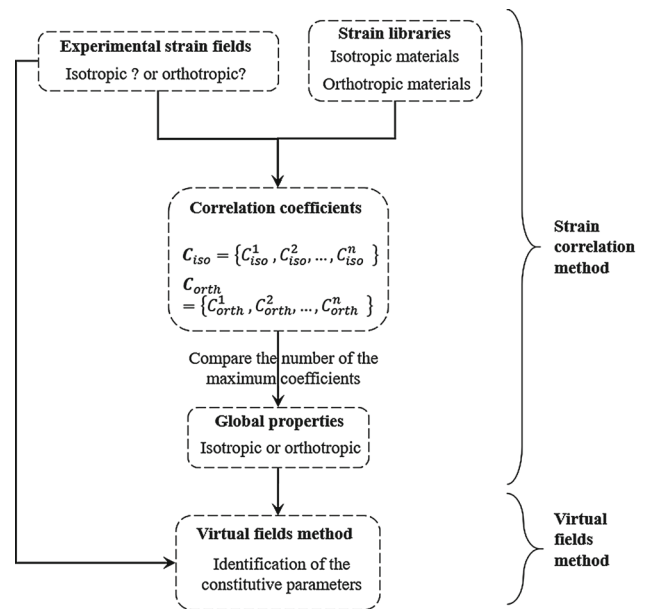


Fig. 3 Flowchart of the SCM-VFM

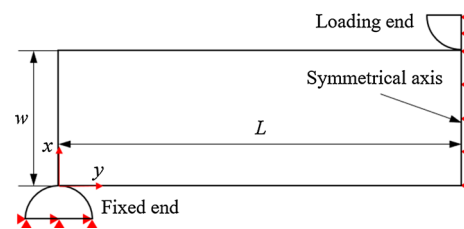
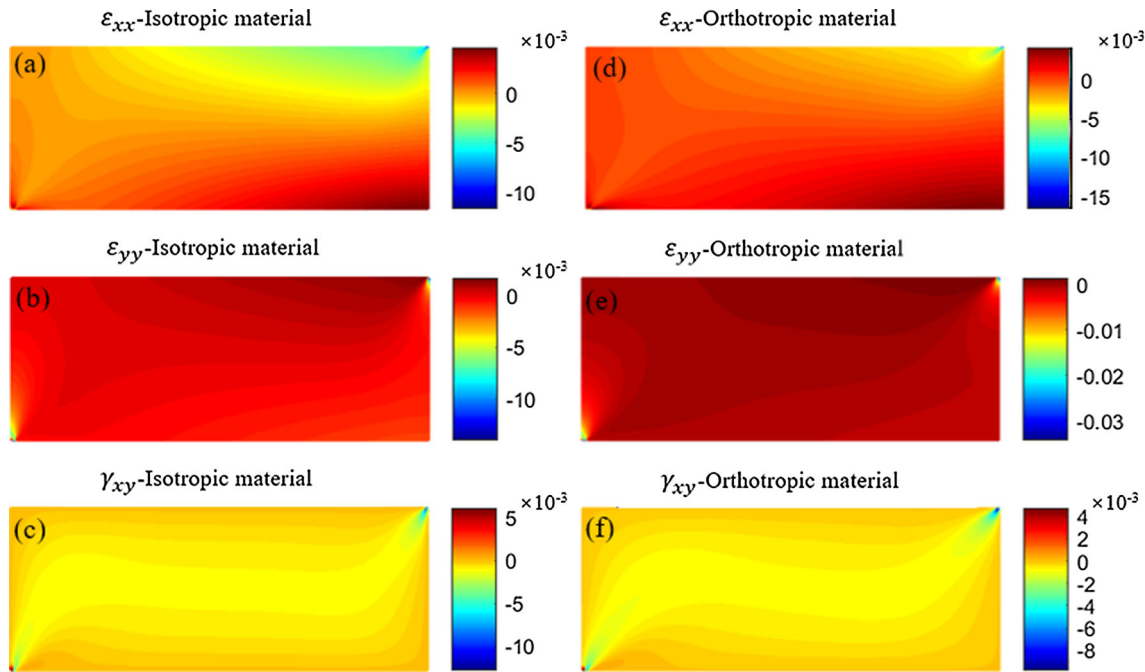


Fig. 4 Three-point bending model in ABAQUS

strain fields conveniently and quickly. To ensure the correctness of the SCM, the samples in the strain library should be as many as possible, but too many samples may increase the amount of calculation. In this study, the number of samples n in each strain library is 16. Considering Young’s modulus and Poisson’s ratio of common materials, for the isotropic strain library, Young’s modulus is selected as 50 GPa, 100 GPa, 150 GPa, 200 GPa, and the Poisson’s ratio is selected as 0.25, 0.28, 0.31, 0.34. Therefore, there are 16 different materials for the isotropic strain library. For the orthotropic strain library, since the 2-D orthotropic material has four independent engineering constants (E_1, E_2 —Young’s modulus along the material principal axis, ν_{12} —principal Poisson’s ratio, G_{12} —shear modulus), so E_1 is selected as 60 GPa, 190 GPa, E_2 is considered to be smaller than E_1 , and E_2 is set as 20 GPa, 50 GPa. ν_{12} is selected as 0.27, 0.32, and G_{12} is selected as 60 GPa, 110 GPa. Therefore, for the orthotropic strain library, there are also 16 materials. In the numerical experiments, the engineering constants will be converted to the stiffness coefficients (Q_{11}, Q_{22}, Q_{12} , and Q_{66}). It should be noted that the materials in the orthotropic strain library are completely orthotropic, that is, E_1 is not equal to E_2 , or Q_{11}

Table 1 Parameters of simulated materials

Isotropic material			Orthotropic material ($Q_{11} \neq Q_{22}$)				
F/N	E/GPa	ν	F/N	Q_{11}/GPa	Q_{22}/GPa	Q_{12}/GPa	Q_{66}/GPa
983.2	150	0.30	1105.6	185.95	61.98	19.22	90

**Fig. 5** Strain fields of **a** ε_{xx} , **b** ε_{yy} , and **c** γ_{xy} of isotropic material, and strain fields of **d** ε_{xx} , **e** ε_{yy} , and **f** γ_{xy} of orthotropic material

is not equal to Q_{22} . In addition, the principal axis (1–2) of the materials is consistent with the measurement axis (x – y) in the simulation.

Once the parameters in the strain library are determined, the strain fields need to be obtained through ABAQUS and exported to MATLAB for calculations. There are a total of 32 calculations that need to be performed. It will take a long time if it is manually operated. Therefore, this paper has realized automatic calculation through MATLAB–ABAQUS. The calculation process is: the finite element calculation is performed in ABAQUS, and then, by modifying the .inp file and programming with MATLAB codes, the strain fields can be obtained directly in MATLAB. Some MATLAB functions can be found in Refs. [27, 28].

To verify that SCM can determine the material global properties, one kind of isotropic material and one kind of completely orthotropic material ($Q_{11} \neq Q_{22}$) are simulated in ABAQUS. The parameters of the two materials are shown in Table 1. The mesh density is 0.05 mm^{-1} , and the derived strains are the values at the center of the element.

To directly illustrate that SCM is not sensitive to noise, the additive Gaussian white noise with a standard deviation of 0.001 is added to the strain fields in Table 1. The strain fields without noises are shown in Fig. 5. Bring the strain

fields in Fig. 5 to the SCM program to obtain the two groups of correlation coefficients (C_{iso} and C_{c-orth} , subscript “ c - $orth$ ” means completely orthotropic) for each strain field, as shown in Fig. 6. The label (Material ID) of the horizontal axis represents the ID of different material parameters in the strain library.

Figure 6a–c shows that the correlation coefficients between the isotropic material and isotropic strain library are always maximum. Figure 6d–f shows that most of the coefficients between the orthotropic material ($Q_{11} \neq Q_{22}$) and orthotropic strain library ($Q_{11} \neq Q_{22}$) are maximum. In Fig. 6d, f, a total of 12 coefficients indicate that the material is orthotropic, and 4 coefficients indicate that the material is orthotropic. For the misjudgment of 4 values (Materials ID 9–12), it is believed that the correlation calculation of Eq. (1) is not optimal. However, since C_{c-orth} has the largest number of maximum coefficients, the material is determined to be orthotropic. Therefore, it can be concluded that SCM can be used to determine whether the material is isotropic or orthotropic ($Q_{11} \neq Q_{22}$). It should be noted that in the two groups of correlation coefficients, if not all of the values in one group are greater than these in the other group, then the material global properties are determined according to the number of maximum coefficients in C_{iso} and C_{c-orth} .

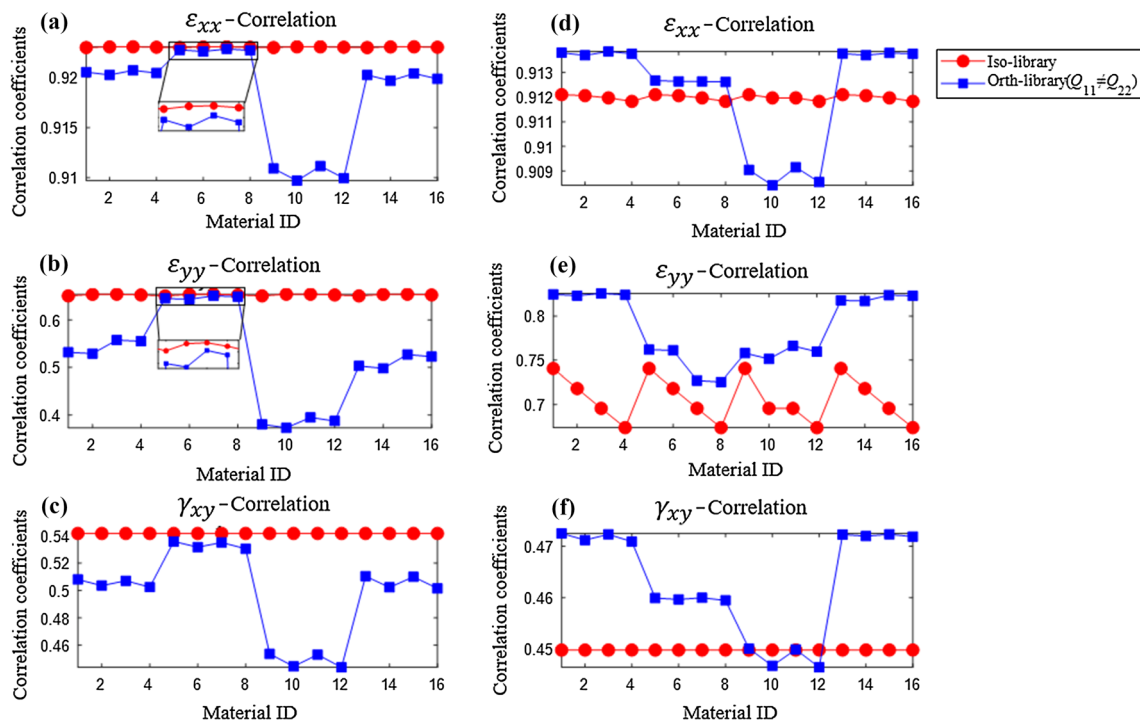


Fig. 6 Correlation coefficients of isotropic strain fields of **a** ϵ_{xx} , **b** ϵ_{yy} , and **c** γ_{xy} with strain libraries, and correlation coefficients of orthotropic strain fields of **d** ϵ_{xx} , **e** ϵ_{yy} , and **f** γ_{xy} with strain libraries

Table 2 Identified parameters using OP-VFM

	Isotropic material		Orthotropic material ($Q_{11} \neq Q_{22}$)			
	Q_{11}/GPa	Q_{12}/GPa	Q_{11}/GPa	Q_{22}/GPa	Q_{12}/GPa	Q_{66}/GPa
Reference	164.84	49.45	185.96	61.99	19.22	90
Identified	166.47	50.06	188.35	63.50	19.74	90.96
Relative error (%)	0.99	1.27	1.29	2.44	2.70	1.06

Finally, the constitutive parameters are identified by the optimized polynomial VFM (OP-VFM). The identified parameters are shown in Table 2.

3.2 Characterization of bidirectional reinforced orthotropic materials

For bidirectional reinforced orthotropic materials ($Q_{11} = Q_{22}$), another orthotropic strain library where Q_{11} and Q_{22} are equal is created. In the same way, E_1 and E_2 are selected as 95 GPa, 125 GPa, 155 GPa, 185 GPa, 215 GPa. ν_{12} is selected as 0.27, 0.32, and G_{12} is selected as 50 GPa, 75 GPa. Hence, there are also 16 materials. Then, one kind of bidirectional reinforced orthotropic material is simulated in ABAQUS. The parameters are shown in Table 3. The additive Gaussian white noise with a standard deviation of 0.001 is also added into the strain fields. In addition to the two strain libraries in Sect. 3.1, there are three strain libraries in total, so three groups of correlation coefficients (C_{iso} , C_{c-orth} , and

Table 3 Parameters of simulated bidirectional reinforced orthotropic materials ($Q_{11} = Q_{22}$)

F/N	Q_{11}/GPa	Q_{12}/GPa	Q_{66}/GPa
1212.4	196.53	56.99	100

C_{b-orth} , subscript “*b-orth*” means bidirectional reinforced orthotropic) for each strain field can be obtained. For simplicity, only the strain field ϵ_{xx} is used for calculation. The correlation coefficients are shown in Fig. 7.

From Fig. 7, it can be seen that the simulated material is not completely orthotropic, and a total of 12 coefficients indicate that the material is bidirectional reinforced orthotropic, and 4 coefficients indicate that the material is isotropic, so the material is considered to be bidirectional reinforced orthotropic ($Q_{11} = Q_{22}$). Therefore, the SCM can determine the material global properties when the material is bidirectional reinforced orthotropic. For the governing equations of VFM are

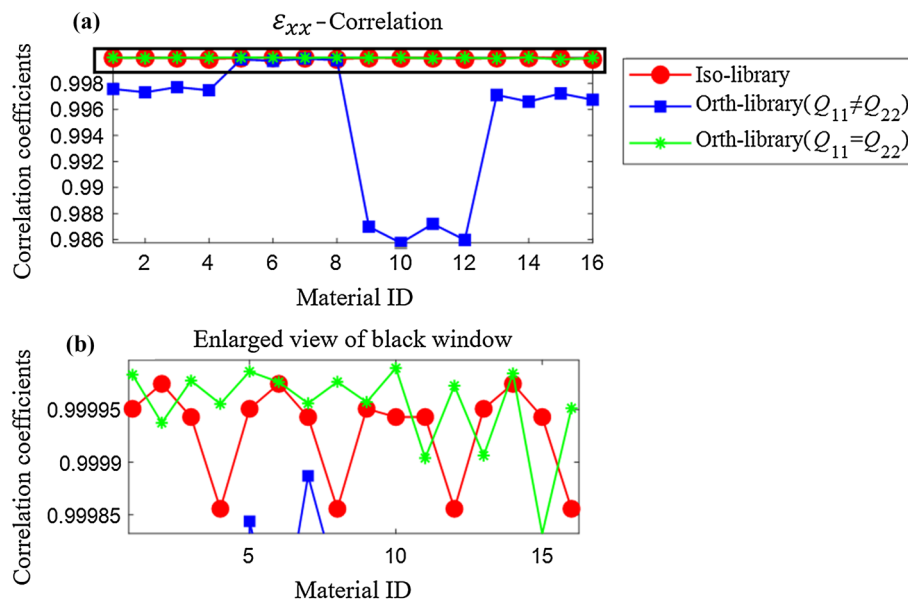


Fig. 7 **a** Correlation coefficients of the bidirectional reinforced orthotropic material with strain libraries and **b** enlarged view of black window

the same (see Eq. (7)), the isotropic VFM can also be used to identify the parameters (Q_{11} , Q_{12} , and Q_{66}).

3.3 Comparison between SCM and orthotropic VFM

Although the orthotropic VFM can be used directly to characterize the material with unknown global properties, as described in the introduction. Nevertheless, because the VFM requires high accuracy of the strain fields, it sometimes may get wrong results in the real experiment, especially when the global properties of the materials are isotropic or bidirectional reinforced orthotropic. In this section, the proposed SCM is compared with orthotropic VFM in terms of the local errors in strain fields and missing data at the specimen edges.

3.3.1 Effect of local errors in strain fields

The above discussions on the strain fields are considering the additive Gaussian white noise. Although the standard deviation is large, it is a homogeneous variance. In real experiments, due to the systematic errors of the measurement technology and various numerical errors, the obtained strain fields may have errors locally, as shown in Fig. 8. The local error in this article is defined as the local fluctuation of the strain field. Figure 8a is the three-point bending strain field (ε_{xx}) in the DIC experiment. It can be seen that there are many fluctuations in the strain field, which is not as smooth as the simulated strain field, as shown in the red window in Fig. 8a. The enlarged view of the red window is shown in Fig. 8b. The values of three characteristic points (A , B , and C) are selected to illustrate the magnitude of the fluctuation. The

values at points A , B , and C are 2.207×10^{-3} , 6.70×10^{-4} , and 7.12×10^{-4} , respectively. Therefore, the magnitude of the fluctuation has reached 10^{-3} . Considering that the magnitude of the fluctuation in the experiment can reach 10^{-3} , to simulate such numerical fluctuations, the Gaussian distribution is used to approximate such fluctuations, as shown in Fig. 8d. The size of the local errors is $2 \text{ mm} \times 2 \text{ mm}$.

To investigate whether the local errors can affect SCM and orthotropic VFM to determine the material global properties, the local errors are added to the isotropic strain fields in Table 1. The final strain fields are shown in Fig. 9. The position of the black box is where the local errors are added.

First, the orthotropic VFM is performed for identification. For comparison, the isotropic VFM is also performed, and the results are shown in Table 4. From the results in Table 4, if the global properties are not determined before using VFM, when there are local errors in the strain fields, directly using orthotropic VFM can get wrong identification results. The error between Q_{11} and Q_{22} cannot be negligible, and it cannot accurately reflect the material mechanical properties. Nevertheless, if the isotropic property can be correctly determined and the isotropic VFM is adopted, the correct parameters can be identified.

Then, the SCM is performed to determine the global properties of the isotropic strain fields in Table 1. The correlation coefficients are shown in Fig. 10. For simplicity, only the comparison results of the strain field ε_{xx} are given here. The isotropic material is compared with the isotropic library and two kinds of the orthotropic library ($Q_{11} \neq Q_{22}$ and $Q_{11} = Q_{22}$). Figure 10 shows that the SCM can successfully

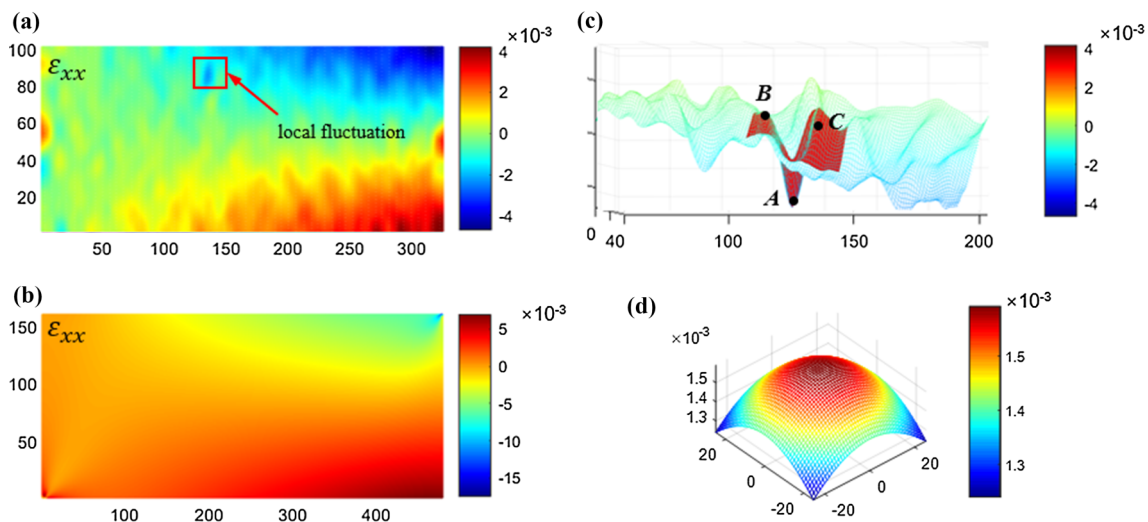


Fig. 8 **a** Experimental strain field. **b** Enlarged view of the red window in **a**. **c** Simulated strain field. **d** Local errors

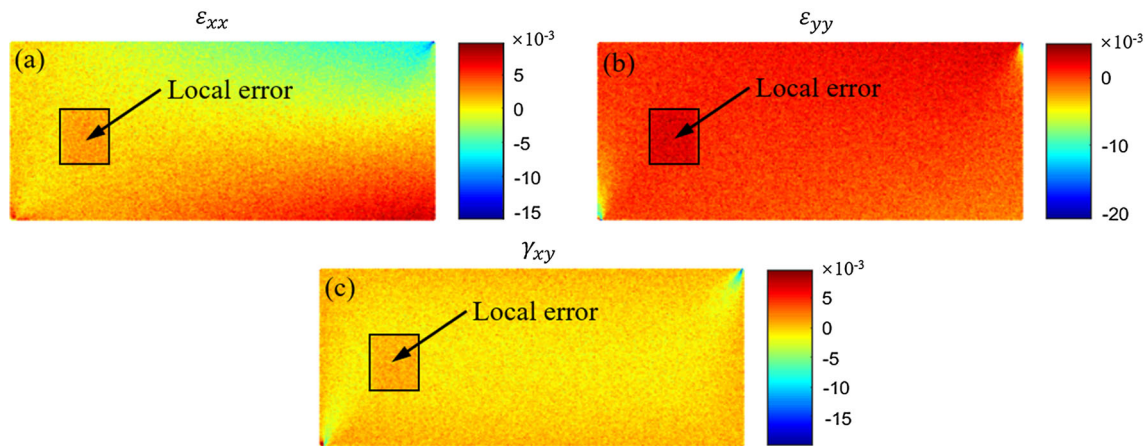


Fig. 9 Strain fields of **a** ϵ_{xx} , **b** ϵ_{yy} , and **c** γ_{xy} with local errors and additive Gaussian white noise

Table 4 Identified parameters using OP-VFM

	Isotropic VFM		Orthotropic VFM			
	Q_{11}/GPa	Q_{12}/GPa	Q_{11}/GPa	Q_{22}/GPa	Q_{12}/GPa	Q_{66}/GPa
Reference	164.84	49.45	164.84	164.84	49.45	57.69
Identified	166.91	48.99	164.85	135.64	40.84	61.32
Relative error (%)	1.26	0.93	0.27	17.71	17.42	6.29

determine the material global properties when there are local errors in strain fields.

3.3.2 Effect of the missing data at the specimen edges

In addition to various noises in the experiment, there is also the problem of missing data at the specimen edges caused by measurement technology. Several studies have shown that the missing data near the edges will seriously affect the accuracy of the identification results [13, 18, 29]. At present, the sim-

plest and most effective way is to add the last row of the data to the edges, and then perform interpolation processing [13].

To investigate whether missing data at the specimen edges can affect SCM and orthotropic VFM to determine the material global properties, the data near the edges of the isotropic material in Table 1 are removed, as shown in Fig. 11a, and the M represents the distance to be removed. The simulation also considers the additive Gaussian white noise with a standard deviation of 0.001.

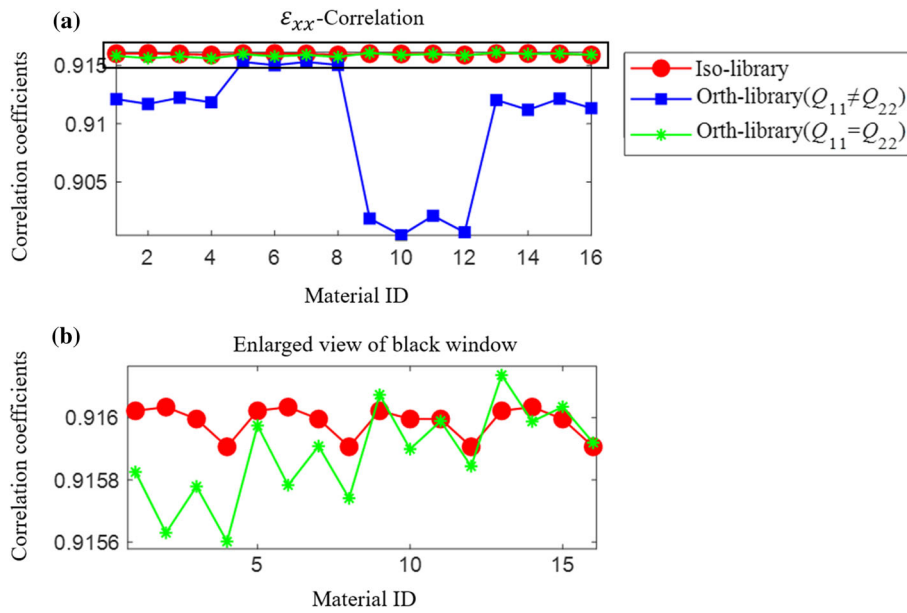


Fig. 10 **a** Correlation coefficients of the isotropic material with strain libraries when considering the local errors and **b** enlarged view of black window

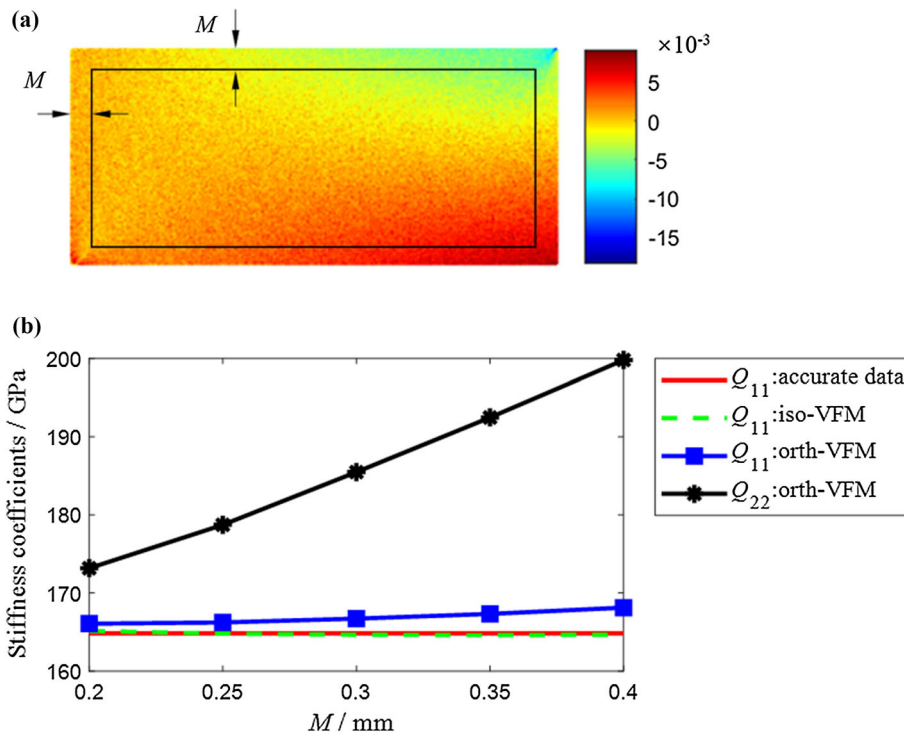


Fig. 11 Missing data at the edges **a** removal settings in simulation, **b** Q_{11} and Q_{22} identified by orthotropic VFM and isotropic VFM

First, the VFM is performed for identification. Before the calculation, the data near the edges was supplemented by linear interpolation. The orthotropic and isotropic VFM are simultaneously performed. The identified Q_{11} and Q_{22} are shown in Fig. 11b.

From the identification results in Fig. 11b, if the orthotropic VFM is directly performed, even if the interpolation near the edges has been adopted, the difference between Q_{11} and Q_{22} is not negligible. In that case, the mechanical properties will be wrongly determined. However, the isotropic VFM can still obtain reasonable parameters, so it is

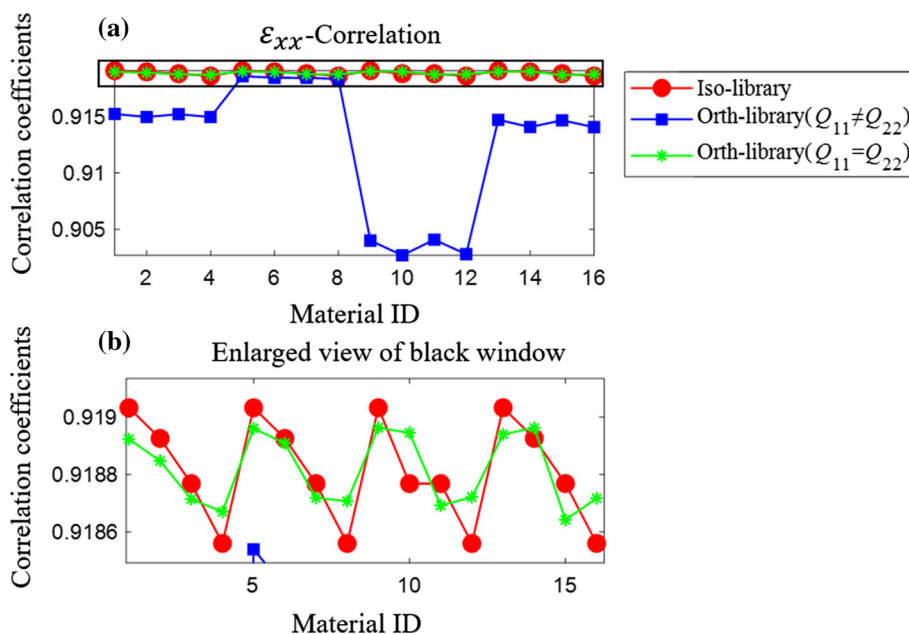


Fig. 12 **a** Correlation coefficients of the isotropic material with strain libraries when considering missing data at the specimen edges and **b** enlarged view of black window

very important to determine the global property before using VFM.

Then, the SCM is performed to determine the material global properties considering missing data at the specimen edges. Similarly, the data near the edges is supplemented by linear interpolation before the calculation. The correlation coefficients are shown in Fig. 12. The same conclusion as in Sect. 3.3.1 can be obtained. Using SCM can successfully determine the global properties when considering the missing data at the specimen edges.

This section shows that SCM does not require high accuracy of the strain fields when determining the global properties compared with that using the orthotropic VFM, and for SCM, the material global properties can be determined by using only one strain field. Determining the material global properties is an important step before the parameter identification, which will bring many conveniences for the calculation using VFM, such as the determination of the number of unknown parameters and the selection of the virtual fields, especially for the isotropic or bidirectional reinforced orthotropic materials. Furthermore, four-parameter identification using orthotropic VFM requires the measured strain fields to be more accurate than that of isotropic VFM. Therefore, before using the VFM, constitutive behaviors or global properties should be determined. This is the significance of developing SCM.

4 DIC experiments

The simulation experiments are always ideal. To further illustrate the feasibility of SCM in real experiments, two experiments are conducted in this section. The first is a verification experiment, which will characterize the PMMA (known as the isotropic material). The second is an application experiment, which will characterize the Ti-6Al-4V alloys (unknown global properties) fabricated by selective laser melting (SLM).

To measure the strain fields of the three-point bending configuration, DIC technique is utilized. The experiment setup is shown in Fig. 13. The resolution of the 8-bit CMOS used in this work is 1280 × 1024. The DIC calculation is conducted by the open-source 2D-DIC MATLAB program, Ncorr, developed by Justin Blaber of Georgia Institute of Technology [30]. The displacement and strain resolutions are 2.6 μm and approximately 1.2 × 10⁻⁴, respectively. The bilateral telecentric lens is used to reduce the influence of the out-of-plane displacements [31].

4.1 PMMA experiment

The PMMA specimen captured by CMOS is shown in Fig. 14a, and the red window is the area of interest (AOI). Figure 14b is an enlarged part of the blue window in Fig. 14a, and the speckle patterns on the surface can be observed. Due to symmetry, only half of the specimen is calculated. The subset radius for calculating the displacement is 18 pixels according to the DIC guide [32], the step size is 2 pixels, and

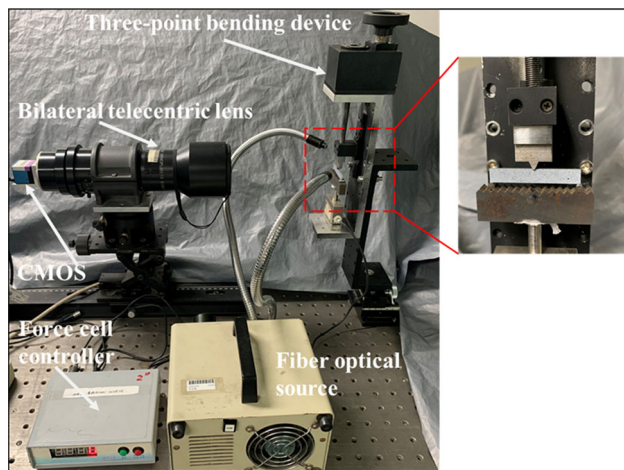


Fig. 13 Experimental setup

the step size should not be too large, otherwise, the identification errors will increase [13]. The strain window radius is 8 pixels or 14 pixels. The strain fields when the strain window radius is 14 pixels are shown in Fig. 15.

4.2 Application in SLM-fabricated Ti-6Al-4V alloys

The SLM-fabricated Ti-6Al-4V alloys used in this paper were manufactured by Wuhan Huake 3-D Technology Co. Ltd.,

China (Huake 3-D HKM125). To explore the effect of the fabricating routes on the mechanical properties of the Ti-6Al-4V alloys, we have designed two kinds of fabricating schemes, as shown in Fig. 16. The first kind is to fabricate the materials in the x -direction first, and then change the direction along the y -axis when fabricating the next layer, as shown in Fig. 16a. The second one is to fabricate the materials along the positive angle of 135° with the x -axis, and then change the direction along the positive angle of 45° with the x -axis, as shown in Fig. 16b.

The Ti-6Al-4V specimen captured by CMOS is shown in Fig. 17. The subset radius for calculating the displacement is 18 pixels, the step size is 2 pixels, and the strain window radius is 11–15 pixels. The strain fields when the strain window radius is 15 pixels are shown in Fig. 18.

5 Results and discussion

5.1 SCM-VFM results of PMMA

Before performing the SCM calculation, the strain fields obtained in Sect. 4.1 are first interpolated to maintain the same dimensions as those in the strain library. The size of the strain fields in the strain library is 160 rows and 480 columns, and the experimental strain fields are calculated to

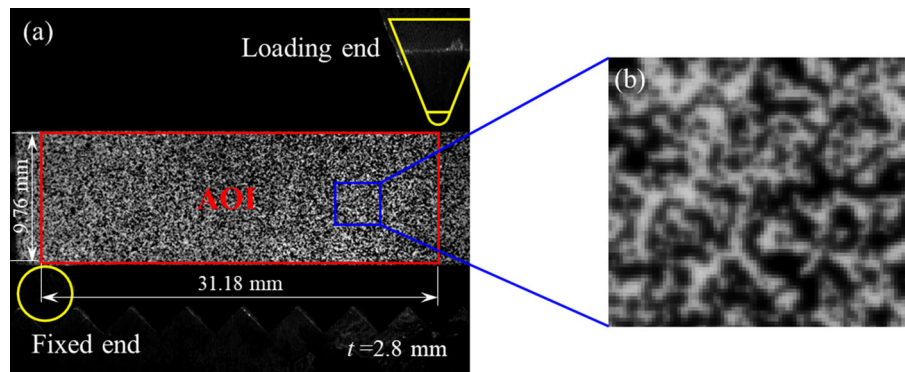


Fig. 14 a PMMA captured by CMOS and b the speckle patterns

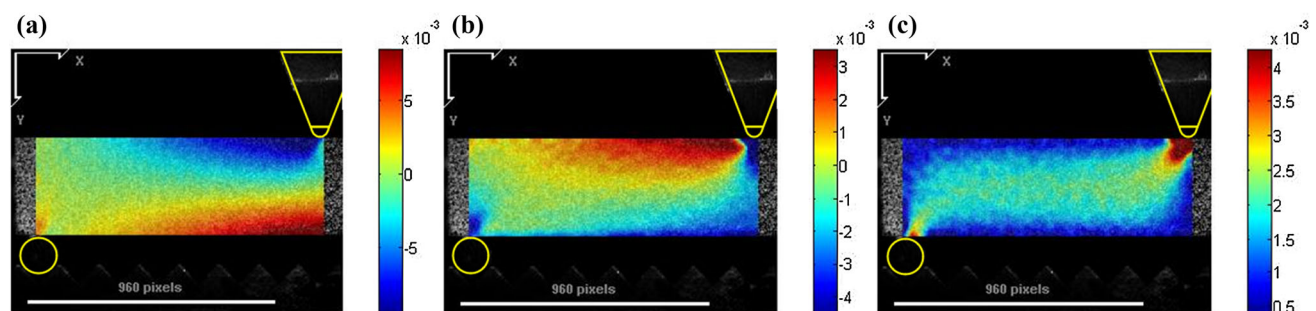


Fig. 15 Strain fields of a ε_{xx} , b ε_{yy} , and c γ_{xy} of PMMA with a load of 102 N

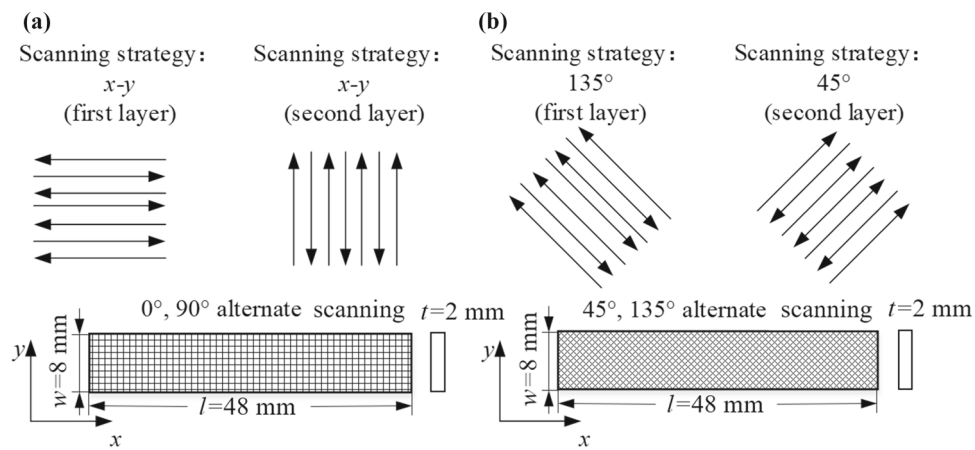


Fig. 16 Fabricating schemes of the SLM specimens: a $0^\circ/90^\circ$ scanning strategy and b $45^\circ/135^\circ$ scanning strategy

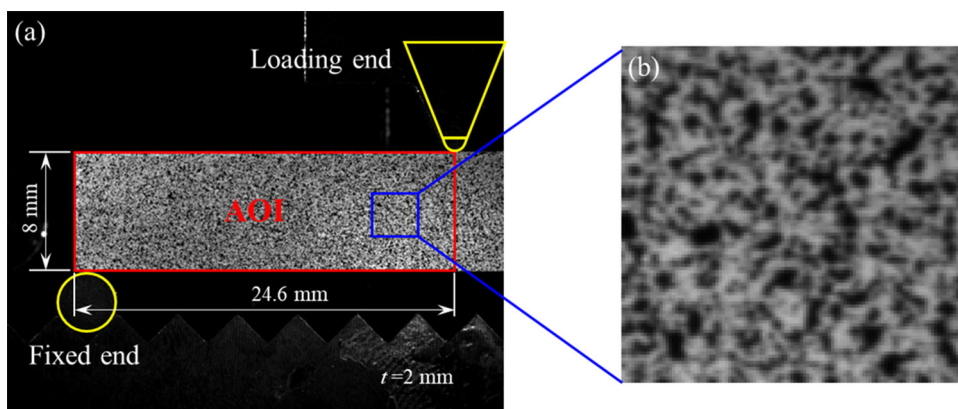


Fig. 17 a SLM-fabricated specimen captured by CMOS and b the speckle patterns

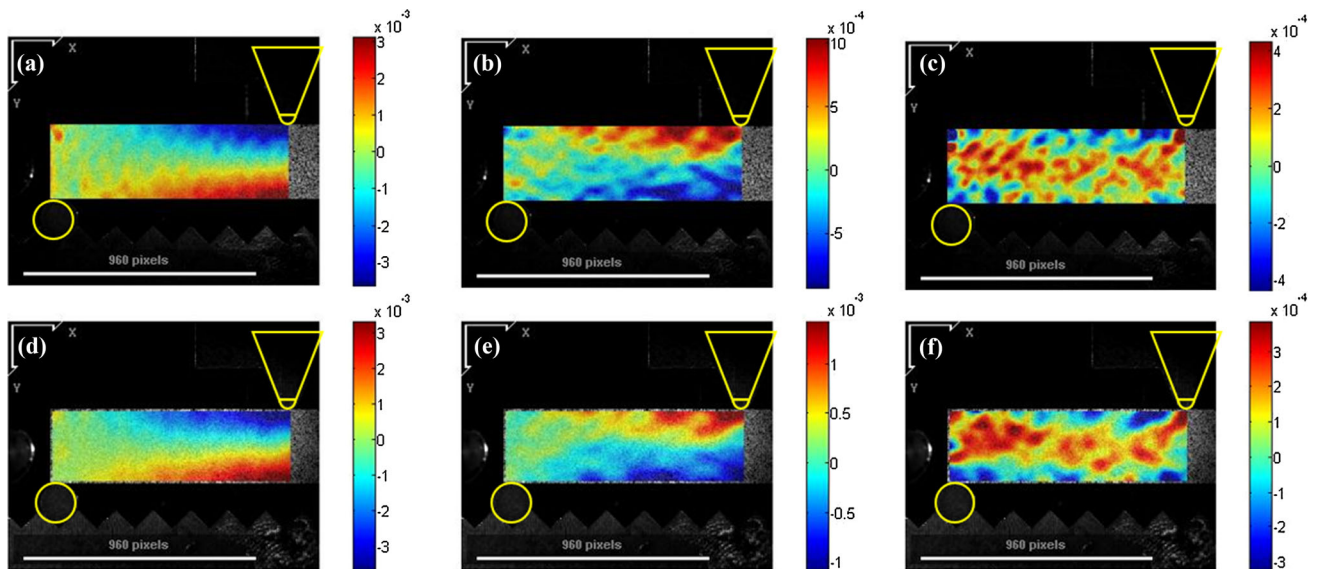


Fig. 18 Strain fields of a ϵ_{xx} , b ϵ_{yy} , and c γ_{xy} of $0^\circ/90^\circ$ specimen with a load of 900 N, and strain fields of d ϵ_{xx} , e ϵ_{yy} , and f γ_{xy} of $45^\circ/135^\circ$ specimen with a load of 962 N

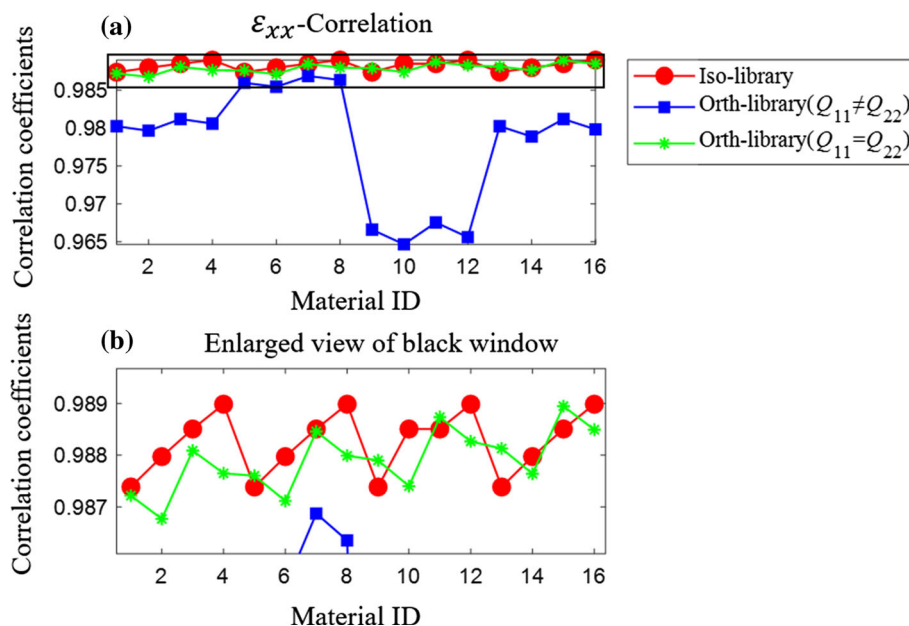


Fig. 19 Correlation coefficients of the PMMA: **a** compared with the isotropic library and two kinds of the orthotropic library ($Q_{11} \neq Q_{22}$ and $Q_{11} = Q_{22}$) and **b** enlarged view of the black window

be 132 rows and 379 columns. The SCM results are shown in Fig. 19.

Figure 19 shows that the PMMA is not completely orthotropic ($Q_{11} \neq Q_{22}$), and a total of 11 coefficients indicate that it is isotropic, and 5 coefficients indicate that it is bidirectional reinforced orthotropic ($Q_{11} = Q_{22}$), so it can be concluded that it is isotropic. The results are consistent with what we know, so SCM can determine the material global properties in the real experiment.

Finally, the isotropic VFM and orthotropic VFM are performed to identify the constitutive parameters. Even though we already know that PMMA is an isotropic material, here we also use orthotropic VFM. The purpose is to show that for isotropic materials, using orthotropic VFM (four-parameter identification) could get wrong identification results. The identification results are shown in Table 5. From the results using orthotropic VFM in Table 5, the error between Q_{11} and Q_{22} is not negligible, that is to say, it cannot be concluded the material is isotropic, which is unreasonable for PMMA. When isotropic VFM is used for identification, the obtained Young's modulus and Poisson's ratio are 3.03 GPa and 0.388, respectively, which are reasonable results compared with Ref. [11].

5.2 Results and analysis of the SLM-fabricated alloys

5.2.1 SCM results of the SLM-fabricated alloys

For the SLM-fabricated alloys, to make the spindle of the sample material consistent with the spindle of the finite ele-

ment model, the strain field ε_{xx} of the $0^\circ/90^\circ$ specimen is used for SCM in this section, and the SCM results are shown in Fig. 20.

The results in Fig. 20a, c show that the $0^\circ/90^\circ$ specimen is not completely orthotropic. In Fig. 20b, d, a total of 11 coefficients indicate that it is isotropic, and 5 coefficients indicate that it is bidirectional reinforced orthotropic ($Q_{11} = Q_{22}$), so it can be concluded that it is isotropic. The same conclusion can be found in Ref. [33], which is obtained by observing the microstructure of the material through a micrograph. The alternative cross routes make the grains more equiaxed, which make the microstructure tend to be isotropic. Therefore, it can be known that the $45^\circ/135^\circ$ specimen is also isotropic.

Using the SCM, it can be concluded that the specimens fabricated by alternative cross routes are not orthotropic materials, which means that the number of unknown parameters is not four, but two. In the next section, the $45^\circ/135^\circ$ specimen and VFM are used to show that the Ti-6Al-4V alloys fabricated by alternative cross routes are indeed isotropic.

5.2.2 VFM results of the SLM-fabricated alloys

Both isotropic and bidirectional reinforced orthotropic materials can be characterized using the isotropic VFM in this paper (see Eq. (7)). First, the $45^\circ/135^\circ$ specimen is utilized to determine whether the material tends to be isotropic or bidirectional reinforced orthotropic. For the $45^\circ/135^\circ$ specimen, if it is considered as an orthotropic material, there is an

Table 5 Identified parameters of PMMA

Load/N	Strain window radius (pixels)	Isotropic VFM		Orthotropic VFM			
		Q_{11} /GPa	Q_{12} /GPa	Q_{11} /GPa	Q_{22} /GPa	Q_{12} /GPa	Q_{66} /GPa
51	4	3.55	1.40	2.92	0.62	0.28	0.50
	7	3.60	1.38	2.93	0.68	0.31	0.49
102	4	3.66	1.44	3.00	0.85	0.39	0.61
	7	3.68	1.43	3.00	0.93	0.42	0.61
132	4	3.47	1.34	2.92	0.97	0.43	0.66
	7	3.50	1.35	2.93	1.07	0.47	0.65
Average	–	3.58	1.39	2.95	0.85	0.38	0.59

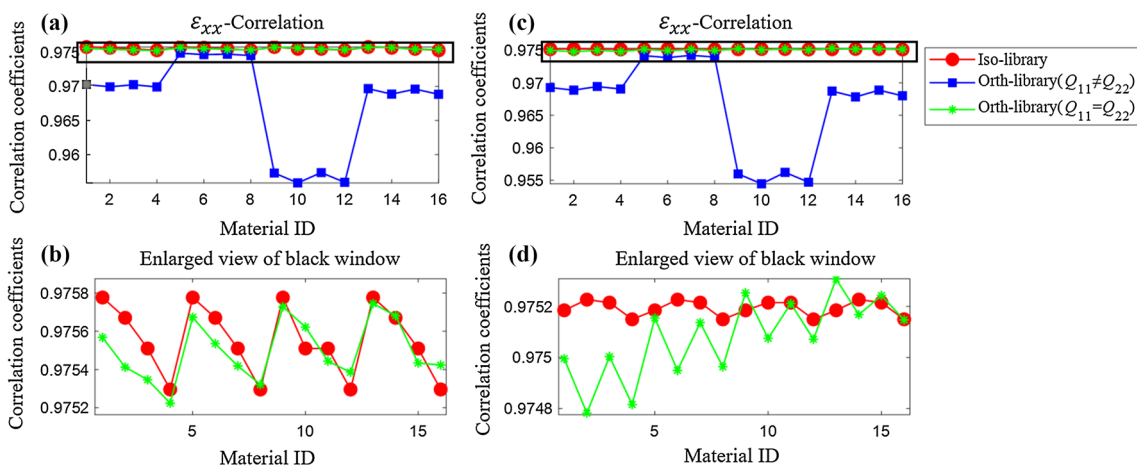


Fig. 20 a, b Correlation coefficients with the load of 760 N. c, d Correlation coefficients with the load of 900 N

angle of 45° between the principal axis (1–2) and the measurement coordinate axis (x – y). Therefore, the strain fields in Fig. 18d–f, and virtual strain fields should be converted to the principal axis. For comparison, the identification results under the measurement coordinate axis (x – y) are also listed, as shown in Table 6. Set-1 and Set-2 indicate that the subset radius is 15 pixels and 18 pixels, respectively. Both the step size and strain radius are 2 pixels and 15 pixels.

The results under the principal axis are very unreasonable, which are compared with Young’s modulus in Refs. [34, 35]. Besides, the Poisson’s ratio is also very unreasonable. From the results in the x – y coordinate axis, the values of Young’s modulus and Poisson’s ratio are reasonable. The VFM results show that the alloys fabricated by alternative cross routes are isotropic, rather than bidirectional reinforced orthotropic. Through the identification results of the 45°/135° specimen, the same conclusion can be drawn as in Sect. 5.2.1, and finally, the isotropic VFM can be utilized to identify all the parameters. The comparison results of the two kinds of specimens are shown in Fig. 21.

Figure 21 shows a comparison of Young’s modulus, Poisson’s ratio, and shear modulus of the two kinds of specimens

Table 6 Identified results of 45°/135° specimen

Load/N	(1–2) axis		(x–y) axis	
	E /GPa	ν	E /GPa	ν
740				
Set-1	522.57	– 2.156	107.91	0.364
Set-2	516.82	– 2.090	109.01	0.367
801				
Set-1	554.22	– 2.271	109.12	0.362
Set-2	579.37	– 2.391	109.77	0.364
900				
Set-1	460.69	– 1.825	105.19	0.366
Set-2	462.20	– 1.819	106.02	0.367

under different DIC calculation conditions. In Fig. 21, the average Young’s modulus of the 0°/90° specimen and the 45°/135° specimen are 107.95 GPa, 107.01 GPa, the Poisson’s ratio is 0.292, 0.359, and the average shear modulus is 41.08 GPa and 39.36 GPa, respectively. The direct errors of these parameters and the values in the literature are shown in

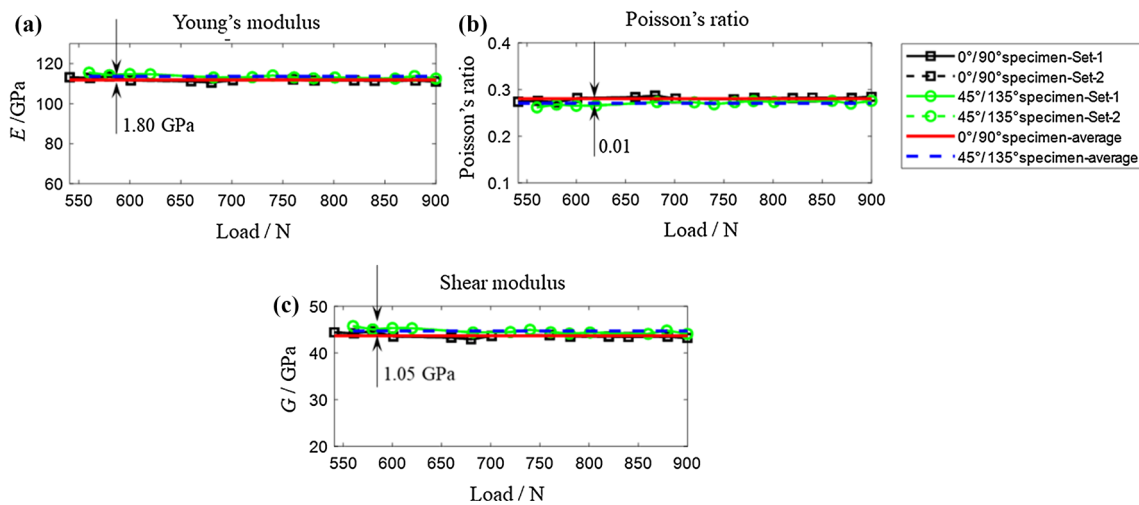


Fig. 21 Comparison of identified results of two kinds of specimens: **a** Young's modulus, **b** Poisson's ratio, and **c** shear modulus

Table 7 Comparison with the results in Refs. [34, 35]

	E/GPa	ν	G/GPa
0°/90° specimen	107.95 ± 4.94	0.292 ± 0.030	41.80 ± 2.40
45°/135° specimen	107.01 ± 2.89	0.359 ± 0.008	39.36 ± 1.06
Ref. [34]	113 ± 5	–	–
Ref. [35]	109.2 ± 3.1	–	–

Table 7. The Young's modulus of the two materials is very close, but the Poisson's ratio is quite different. On the one hand, it is related to the individual difference of the specimen, on the other hand, the experimental conditions, such as speckle quality and lighting conditions, cannot be completely consistent.

In summary, for materials with unknown constitutive behaviors, if they are determined to be isotropic or bidirectional reinforced orthotropic, using SCM can reduce the number of unknown parameters compared with the assumption of complete anisotropy, which will provide a great convenience for identification. For VFM, it can improve the identification capability and the credibility of the results. Besides, for iterative methods such as FEMU, it can also reduce a lot of calculation time.

6 Conclusions

For materials with unknown global properties, the orthotropic VFM can be directly used to identify the material parameters. Unfortunately, the original characterization using this method may lead to wrong identification results. In order to improve the parameter identification ability using VFM, the SCM was proposed to determine the material

global properties before performing the VFM. The following conclusions are obtained.

1. To identify the material parameters when the global properties are unknown, the measured strain fields are correlated with the strain libraries based on the three-point bending configuration. According to the number of the maximum values among the three groups of correlation coefficients (C_{iso} , C_{c-orth} , C_{b-orth}) the material global properties can be determined. The proposed method can improve the credibility of identification results using VFM.
2. The feasibility and accuracy of the SCM are verified using simulations and real experiments using PMMA. The results indicate that the SCM has good noise immunity and is insensitive to the local errors in the strain fields. Besides, for the missing data at the specimen edges, after the interpolation process, there is no effect on the characterization results of SCM.
3. The proposed SCM is compared with the orthotropic VFM in the determination of the material global properties. The results show that SCM has better robustness.
4. The global properties of the Ti-6Al-4V alloys fabricated by SLM can be successfully characterized by SCM. The results indicate the Ti-6Al-4V alloys fabricated by alternative cross routes are isotropic, and the identified material parameters using isotropic VFM are reasonable compared with those in the literature.

Acknowledgements This research was financially supported by the National Key Research and Development Program of China (Grant 2017YFB1103900), the National Science and Technology Major Project (Grant 2017-VI-0003-0073), the National Natural Science Foundation of China (Grant 11672153), and Hubei Provincial Major Program of Technological Innovation (Grant 2017AAA121).

References

1. Stéphane, A., Bonnet, M., Bretelle, A.S.: Overview of identification methods of mechanical parameters based on full-field measurements. *Exp. Mech.* **48**(4), 381–402 (2008)
2. Martins, J.M.P., Andrade-Campos, A., Thuillier, S.: Comparison of inverse identification strategies for constitutive mechanical models using full-field measurements. *Int. J. Mech. Sci.* **145**, 330–345 (2018)
3. Bruno, L.: Mechanical characterization of composite materials by optical techniques: a review. *Opt. Laser Eng.* **104**, 192–203 (2018)
4. Clément, T., Magnain, B., Serra, Q.: Accuracy and robustness analysis of geometric finite element model updating approach for material parameters identification in transient dynamic. *Int. J. Comput. Methods* **16**(1), 66–78 (2019)
5. Zhu, R.H., Zhang, Q., Xie, H.M.: Determination of residual stress distribution combining slot milling method and finite element approach. *Sci. China Technol. Sci.* **61**(7), 965–970 (2018)
6. Ladeveze, P., Leguillon, D.: Error estimate procedure in the finite element method and applications. *SIAM J. Numer. Anal.* **20**(3), 485–509 (1983)
7. Guchhait, S., Banerjee, B.: Anisotropic linear elastic parameter estimation using error in the constitutive equation functional. *Proc. R. Soc. A Math. Phys.* **472**(2192), 20160213 (2016)
8. Claire, D., Hild, F., Roux, S.: A finite element formulation to identify damage fields: the equilibrium gap method. *Int. J. Numer. Methods Eng.* **61**(2), 189–208 (2004)
9. Mei, Y., Avril, S.: On improving the accuracy of nonhomogeneous shear modulus identification in incompressible elasticity using the virtual fields method. *Int. J. Solids Struct.* **178**, 136–144 (2019)
10. Mei, Y., Goenezen, S.: Quantifying the anisotropic linear elastic behavior of solids. *Int. J. Mech. Sci.* **163**, 105131 (2019)
11. Pierron, F., Grédiac, M.: *The Virtual Fields Method: Extracting Constitutive Mechanical Parameters from Full-field Deformation Measurements*. Springer, New York (2012)
12. Grédiac, M., Pierron, F., Avril, S.: The virtual fields method for extracting constitutive parameters from full-field measurements: a review. *Strain* **42**(4), 233–253 (2006)
13. Rossi, M., Lava, P., Pierron, F., et al.: Effect of DIC spatial resolution, noise and interpolation error on identification results with the VFM. *Strain* **51**(3), 206–222 (2015)
14. Zhou, M., Xie, H., Wu, L.: Virtual fields method coupled with moiré interferometry: special considerations and application. *Opt. Laser Eng.* **87**, 214–222 (2016)
15. Badulescu, C., Grédiac, M., Mathias, J.D.: A procedure for accurate one-dimensional strain measurement using the grid method. *Exp. Mech.* **49**, 841–854 (2009)
16. Avril, S., Pierron, F.: General framework for the identification of constitutive parameters from full-field measurements in linear elasticity. *Int. J. Solids Struct.* **44**(14–15), 4978–5002 (2007)
17. Bai, R., Jiang, H., Lei, Z.: Virtual field method for identifying elastic-plastic constitutive parameters of aluminum alloy laser welding considering kinematic hardening. *Opt. Laser Eng.* **110**, 122–131 (2018)
18. Dai, X., Xie, H.: Constitutive parameter identification of 3D printing material based on the virtual fields method. *Measurement* **59**, 38–43 (2015)
19. Cao, Q., Xie, H.: Characterization for elastic constants of fused deposition modelling-fabricated materials based on the virtual fields method and digital image correlation. *Acta Mech. Sin.* **33**(6), 1075–1083 (2017)
20. Zhou, M.M., He, W., Xie, H.M., et al.: Characterization of mechanical properties of 3-D printed materials using the asymmetric four-point bending test and virtual fields method. *J. Test. Eval.* **49**(1), 20180598 (2021)
21. Renee, M., Arunark, K., Martyn, P.N.: Estimation of transversely isotropic material properties from magnetic resonance elastography using the optimised virtual fields method: estimation of transversely isotropic material properties from MRE. *Int. J. Numer. Methods Biomed.* **34**(6), e2979 (2017)
22. Yunquan, S., Xuefeng, Y., Shen, W.: Simultaneous determination of virtual fields and material parameters for thermo-mechanical coupling deformation in orthotropic materials. *Mech. Mater.* **124**, 33–44 (2018)
23. Avril, S., Grédiac, M., Pierron, F.: Sensitivity of the virtual fields method to noisy data. *Comput. Mech.* **34**(6), 439–452 (2004)
24. Grédiac, M., Pierron, F.: Numerical issues in the virtual fields method. *Int. J. Numer. Methods Eng.* **59**(10), 1287–1312 (2004)
25. Pierron, F., Vert, G., Burguete, R.: Identification of the orthotropic elastic stiffnesses of composites with the virtual fields method: sensitivity study and experimental validation. *Strain* **43**(3), 250–259 (2007)
26. Smouse, P.E., Long, J.C.: Matrix correlation analysis in anthropology and genetics. *Am. J. Phys. Anthropol.* **35** (Supplement S15), 187–213 (1992)
27. Papazafeiropoulos, G., Muñoz-Calvente, M., Martínez-Pañeda, E.: Abaqus2Matlab: a suitable tool for finite element post-processing. *Adv. Eng. Softw.* **105**, 9–16 (2017)
28. Papazafeiropoulos, G.: Abaqus2Matlab (<https://www.mathworks.com/matlabcentral/fileexchange/54919-abaqus2matlab>), MATLAB Central File Exchange. (2020)
29. Jiang, L., Guo, B., Xie, H.: Identification of the elastic stiffness of composites using the virtual fields method and digital image correlation. *Acta Mech. Sin.* **31**(02), 173–180 (2015)
30. Blaber, J., Adair, B., Antoniou, A.: Ncorr: open-source 2D digital image correlation Matlab software. *Exp. Mech.* **55**, 1105–1122 (2015)
31. Wu, L., Zhu, J., Xie, H.: Single-lens 3D digital image correlation system based on a bilateral telecentric lens and a bi-prism: validation and application. *Appl. Opt.* **54**(26), 7842–7850 (2015)
32. Jones, E.M.C., Iadicola, M.A.: *A Good Practices Guide for Digital Image Correlation*. In: *International Digital Image Correlation Society*. Springer, New York (2018). <https://doi.org/10.32720/idics/gpg.ed1>
33. Thijs, L., Verhaeghe, F., Craeghs, T.: A study of the microstructural evolution during selective laser melting of Ti-6Al-4V. *Acta Mater.* **58**(9), 3303–3312 (2010)
34. Simonelli, M., Tse, Y.Y., Tuck, C.: Effect of the build orientation on the mechanical properties and fracture modes of SLM Ti-6Al-4V. *Mater. Sci. Eng. A Struct.* **616**, 1–11 (2014)
35. Bey, V., Lore, T., Jean-Pierre, K., et al.: Heat treatment of Ti6Al4V produced by selective laser melting: microstructure and mechanical properties. *J. Alloy. Compd.* **541**, 177–185 (2012)

Publisher's Note Springer Nature remains neutral with regard to jurisdictional claims in published maps and institutional affiliations.